

# Modelling of breaking wave dynamics, surf zone turbulence and wave-induced mean flows with the SPH numerical method

Christos Makris<sup>1</sup>, Constantine Memos<sup>2</sup> and Yannis Krestenitis<sup>3</sup>

## Abstract

Continuing our previously published work, plunging wave breaking over relatively mild sloping beach-type formations is investigated in this paper. Numerical modeling aspects on the matter are discussed, by pursuing comparisons against experimental data. The modern robust method Smoothed Particle Hydrodynamics is used and the recently enhanced version of the academic 'open source' code SPHysics v.2 is being validated. Spatial resolution is discerned as the most crucial factor in forming plausible results. Exquisite visual representation of the violent free-surface deformations is further upheld by coincidence of numerical and experimental results of classic and sophisticated flow characteristics, in terms of wave heights, ensemble-averaged values of hydrodynamic features, Fourier spectral analysis of turbulent velocities, vorticity patterns and wave-induced mean flows. Further need to verify the model's ability to capture the near-shore wave breaking dynamics and surf/swash zone turbulence sets the path of future research, based on extremely refined simulations with a new 'parallel' version of SPHysics.

*Keywords: SPH, numerical modelling, wave breaking, plunging, spatial discretization, Smagorinsky, wave height, ensemble-average, surf zone, turbulence, Fourier spectra, vorticity, undertow, Stokes drift*

## 1 Introduction

The evolution of near-shore waves and the consequent shaping of the surrounding hydrodynamic field have traditionally been of major concern for coastal engineers and scientists. Particularly the wave breaking, with its extremely complicated mechanisms, distinguishes among other relevant coastal processes for lack of exhaustive elucidation. The detailed description of the surf zone wave pattern, the consequent turbulent flow characteristics and the wave-induced near-shore currents demand nowadays the use of enhanced computational approaches. Following our previously published research work (Makris et al., 2009; 2010a; 2010b) on the subject, we pursue in the present paper the improvement of our investigations by incorporating newer, more elaborate versions of computational models.

The precise numerical simulation of the solely nonlinear process of plunging wave breaking on plane and relatively mild impermeable slopes, in terms of wave height, free-surface elevation and velocity field persists as the primary aim of our research effort. In addition we focus on the simulation of the wave-induced mean flows in the surf zone, namely the cross-shore return-type flow called the undertow and the shoreward mass transport flow called the Stokes drift. Several other surf and swash zone features such as the mean free-surface elevation (wave setup) and run-up on a mildly sloping beach-type profile are derived as well. Moreover a detailed description of the difficult to obtain turbulent features such as the coherent turbulent structures, the vortical recurring patterns and the power spectra of the fluctuating components of the Eulerian velocity field inside the surf and swash zones is pursued. Finally a wide range of computational simulation results, describing thoroughly the turbulent surf and swash zone features not yet approachable by classic wave models, is presently introduced. All of the above

---

<sup>1</sup> Aristotle University of Thessaloniki, Laboratory of Maritime Engineering and Maritime Works, Division of Hydraulics and Environmental Engineering, Department of Civil Engineering, Faculty of Engineering, GR-54124, Thessaloniki, Greece, cmakris@civil.auth.gr

<sup>2</sup> National Technical University of Athens, School of Civil Engineering, Laboratory of Harbour Works, Heron Polytechniou 5, GR-15780, Zografos, Athens, Greece, memos@hydro.ntua.gr

<sup>3</sup> Aristotle University of Thessaloniki, Laboratory of Maritime Engineering and Maritime Works, Division of Hydraulics and Environmental Engineering, Department of Civil Engineering, Faculty of Engineering, GR-54124, Thessaloniki, Greece, ynkrest@civil.auth.gr

are attempted by means of one of the most ingenious modern CFD methods for the simulation of hydrodynamic free-surface flows, called Smoothed Particle Hydrodynamics (SPH), as described in detail by Monaghan (2005). Results of SPH simulations in the recent literature, albeit visually impressive, demand urgently creditable verification against circumstantial experimental data (Gómez-Gesteira et al., 2010b). Thus the calibration and the overall capability of a state-of-the-art implementation of the SPH method to predict the details of the entire wave breaking process ensues as the major goal of our research.

## 2 Methodology

SPH is a mesh-free particle method, implementing Lagrange-type approximation for the Navier-Stokes equations, through integral interpolation smoothing functions. Its Lagrangian particle nature allows the unhindered simulation of free-surface flows with strong deformations, such as plunging wave breaking in coastal areas, as thoroughly described by Dalrymple & Rogers (2006). The method's foundational aspect is based on the integral interpolation of any given function  $A(\mathbf{r})$  (scalar or vectorial) in the computational domain and its derivatives that finally leads in discrete notation to:

$$A(\mathbf{r}) = \int A(\mathbf{r}')W(\mathbf{r}-\mathbf{r}',h)d\mathbf{r}' \Rightarrow A(\mathbf{r}) = \sum_j A_j (m_j/\rho_j)W_{ij} \quad (1)$$

with  $h$  smoothing length [m]

$\mathbf{r}, \mathbf{r}'$  arbitrary particle point location, distance between particles respectively [m]

$W(\mathbf{r},h)$  distance varied weighting (bell-shaped) function called kernel ( $W_{ij}$  in particle notation)

$m_j, \rho_j$  mass, density of particle  $j$  respectively [kgr, kgr/m<sup>3</sup>]

In-depth analysis of the SPH method can be found in Monaghan (2005) and crucial assumptions of the present implementation of the method can be traced in our previously published work (Makris et al., 2009) as well as in Gómez-Gesteira et al. (2010b).

### 2.1 SPHysics model

Proceeding further, in the ongoing framework of our former research analysis (Makris et al., 2009; 2010a;b), the recent series (launched in sectional work packages in 2010) of the academic 'open source' numerical code SPHysics v.2 (Gómez-Gesteira et al., 2010a) is used. Basic theoretical assumptions remain unmodified, yet several computational code bugs are corrected and new features are inserted in our analysis as far as numerical schemes and kernel manipulation are concerned. Particularly we hereby use a symplectic time integration algorithm and a cubic-spline kernel, presented thoroughly in Gómez-Gesteira et al. (2010a), instead of a predictor-corrector numerical scheme and a quadratic weighting function implemented previously (Makris et al., 2009). In the latter, thorough calibration of all of the model's significant parameters, namely weighting functions  $W(\mathbf{r},h)$ , smoothing length  $h$ , numerical schemes, time-step  $\Delta t$ , viscosity treatment etc, was attempted separately (see also Makris et al., 2010b). It was found that the spatial resolution  $\Delta x$  and the smoothing length  $h$  are most important in shaping the results. Acceptable agreement was thereby succeeded in terms of wave heights  $H$  and bore front velocities  $U_i$ , for one optimum dimensionless smoothing ratio  $\Delta x/h$ . Nonetheless extended refinement of the SPH particle resolution was not formerly attempted due to high computational cost and lack of robustness for solid boundary treatment in older versions of our simulation efforts. The new version of the SPHysics code and new efficient computer equipment in our laboratory allow us to simulate finer flow scales within reasonable computation times.

As far as treatment of viscosity effects is concerned, we persevere in the use of a Sub-Particle Scale (SPS) Smagorinsky type turbulence closure model incorporating a compressible fluid Favre-type averaging technique for the calculated density (Gómez-Gesteira et al., 2010a), in the likes of Large Eddy Simulation Sub-Grid Scale models used in traditional mesh-based methods. The eddy viscosity assumption (Boussinesq hypothesis) is employed, in the framework of a standard non-dynamic Smagorinsky-type model for the derivation of turbulent eddy viscosity, where the Smagorinsky coefficient  $C_s$  is kept constant throughout the computational domain.

The model is also supported by a Shepard density averaging filter to ensure smoothness of free surface depiction and physically plausible results for the description of the highly nonlinear processes of wave breaking, like plunging, overturning, splash-up and wave impact (Makris et al., 2009). Based on Fourier spectral analysis of the fluctuating turbulent component of the velocity field derived from our simulations, it was previously suggested that the aforementioned SPS model performs plausibly in simulating the effects of isotropic (inertial sub-range) turbulence, up to a frequency of  $f=10\text{Hz}$  (Makris et al., 2010b). On the contrary the model behaved poorly for high power spectrum frequencies. Therefore no scaling law was evident for the small unresolved scale eddies, whose effects are supposed to be simulated by the SPS model. This was relevant to areas inside the surf zone near the free surface, where thick layers of vorticity and strong vorticity gradients are present. Throughout the rest of the water column the aforementioned model's attributes become questionable for even broader frequency band widths, namely for larger scale eddies in the flow field. In spite of that, the use of a previously proposed (Makris et al., 2010a;b) quite arduous dynamic Smagorisky-type turbulence closure model was postponed for future research, until correct calibration of the spatial resolution of the particles in the SPPhysics v.2 model is completed firstly. For the latter to be fulfilled, past experience has shown that the size of the particle discretization  $\Delta x$  should be at least equal or smaller than the integral turbulence length scales of a real flow, whose values are extracted from experimental data.

## 2.2 Experimental and numerical data for comparisons

Following Makris et al. (2009), SPPhysics numerical results are being compared against the experimental output data of Stansby & Feng (2005) [SF05 hereafter], which describe near-shore wave breaking and consequent turbulence transport. The geometric, hydraulic and gauge measurement attributes of the experimental setup used as input data to our numerical wave tank simulations undertaken for validation of SPPhysics v.2 have been previously presented in Makris et al. (2009; 2010a,b). Further detailed descriptions can be found in SF05.

Table 1: Discrete simulation test cases based on spatial resolution  $\Delta x$  and other calibration factors

Test	Case	$\Delta x$ (m)	Caibrated Factor	Test	Case	$\Delta x$ (m)	Caibrated Factor
1	17_a	0.02	$\Delta x/h = 0.77$	7	17_xxx	0.005	$\Delta x/h = 0.77$
2	17_b7	0.02	$\Delta x/h = 0.58$	8	17_xxx2	0.006	$\Delta x/h = 0.77$
3	17_xx	0.015	$\Delta x/h = 0.77$	9	17_xxx3	0.00592	$\Delta x/h = 0.77$
4	17_x	0.01	$\Delta x/h = 0.77$	10	17_xxx3b	0.00632	$\Delta x/h = 0.77$
5	17_xb7	0.01	$\Delta x/h = 0.58$	11	17_xxx3c	0.0061	$\Delta x/h = 0.77$
6	17_xt	0.01	$t_0 = 121 \text{ sec}$ $\Delta x/h = 0.77$	12	17_xxx4	0.004	$\Delta x/h = 0.77$
				13	17_xxx5	0.003	$\Delta x/h = 0.77$

In Table 1 the Test cases employed, based on spatial/particle resolution, are shown. Numerical results according to the progressively refined discretization factors are used in convergence and sensitivity analysis presented below, in terms of inter-comparisons of wave height distributions throughout the whole computational domain including wave propagation, surf and swash zones. The dimensionless smoothing ratio  $\Delta x/h$  is set to default as in our older simulations except two cases (2, 5) where a previously demonstrated optimum value is implemented (Makris et al., 2010b). In Test case 6 a large simulation recording time, involving 50 wave periods, is inserted, in order to trace stability issues about derived output data, especially for turbulent features. The values of Test cases 9-11 hinge upon our analysis above, i.e. about the SPS model's ability to represent reasonably the shear effects for unresolved scales. In SF05 the authors state that the integral turbulence length scales should be estimated to vary from 0.04 to 0.18 of the water depth from the outer to the inner surf zone respectively. Thus their values range from 5.92 to 6.32 mm and from 1.35 to 1.71 cm for the outer to the inner surf zone respectively. In Test cases 9-11 we focus on the former values, for the reason that inner surf zone integral

turbulence length scales have been resolved in past simulations. Predicted wave height and mean free-surface elevation values in that region were satisfactory in our past endeavors (Makris et al., 2010a).

### 3 Results and discussion

Following Makris et al. (2009; 2010a;b), various SPHysics v.2 numerical results, ranging from simple depictions of wave characteristics to more sophisticated representations of turbulent features, are compared below against the respective experimental ones of SF05.

#### 3.1 Depiction of near-shore plunging wave breaking

In Fig.1 a streaming sequence of the instantaneous portrayals for Test 13 numerical results (fine particle resolution) is presented. The weak plunging incident reported in SF05 is astonishingly reproduced permitting fine qualitative agreement between numerical and experimental output. The plunging jet formation is initiated and afterwards overturning and impinging of the sharp water tongue upon the forward trough takes place. Consequently a rebound splash-up follows creating an accompanying free-surface bulge shoreward of the breaking surface roller. The latter constitutes the main mechanism of vorticity generation and enhancement due to turbulent production in wave breaking. Finally a turbulent bore formation is shaped and propagation of it is visually traceable up to the swash region. Colour scale refers to velocity magnitudes, whose maximum values at the propagating crest of the breaking wave are roughly 1.5 times the theoretical value of celerity in shallow water,  $c_t=(g \cdot d)^{1/2}$ . It is slightly higher than the experimental ones, which oddly enough correspond to those for spilling and not for plunging breakers. Referring to spatial discretization calibration, we can observe that the finer analysis certainly invokes higher quality representation of the plunging event.

In Fig.2 graphs are given of the bore front propagation and its transformation to a swashing run-up tongue near the shoreline margin. The unaccounted for discrepancy at the bottom and the coastline due to exaggerated repulsion in solid boundary conditions, depicted in Makris et al. (2009; 2010a), is now vanished. Fine particle resolution, combined with the use of the enhanced SPHysics model version, has addressed the matter, although modelling of friction effects at solid boundaries remain an open issue in SPH simulations.

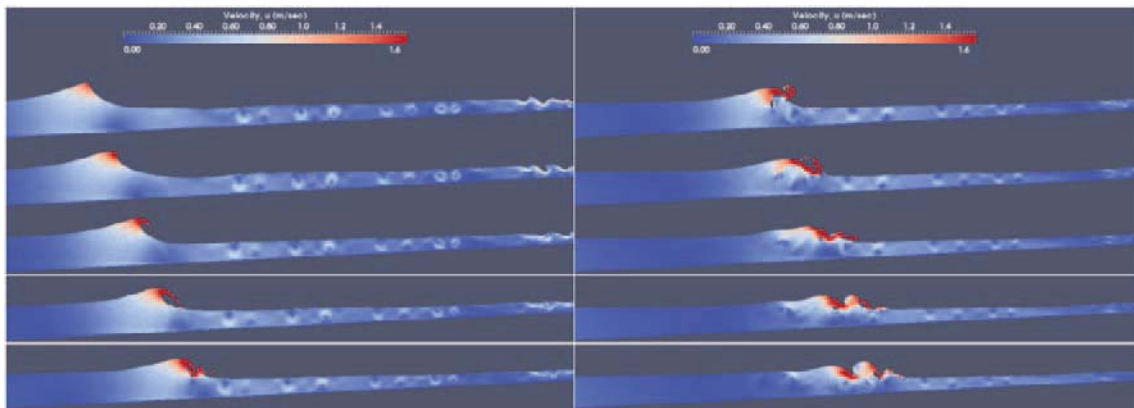


Figure 1: Consecutive captured SPHysics-Paraview output depictions of plunging wave breaking and turbulent bore formation for fine particle resolution

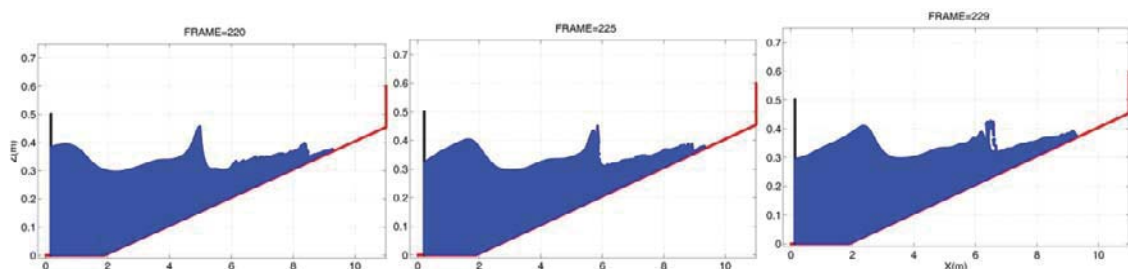


Figure 2: SPHysics-Matlab output frames for plunging wave breaking

### 3.2 Free-surface elevation patterns, wave height and setup

Characteristic free-surface elevation patterns for simulation Test case 13 are presented in Fig.3. Snapshots of the newly refined simulations' free-surface elevation throughout the whole computational domain appear in the upper part. They portray a sensible and stable undular form of the free surface, which appears to be smoother than the respective published in the past. Time-series of free-surface elevation at specific gauge points in crucial regions throughout the examined domain are shown in the lower part of Fig.3. For all of them the oscillation amplitude reaches a steady magnitude within 10 wave periods and that is also the case for the Test case 6, where a larger simulation recording time of 50 periods is taken into account. In Fig.4 (left) comparison of wave height and mean free-surface elevation (wave setup) for Test case 13 is shown. Agreement is reinforced compared to formerly published results, for all cases with spatial discretization equal to  $\Delta x=0.01\text{m}$  and lower. This is valid for both the pre-breaking region and the whole surf/swash zone. Especially in Test case 13 the wave height in the incipient breaking region, where shear effects are intense and the SPS model used to perform poorly, is now closer to the experimental values than any other case. In other regions different resolution may excel more, based on optimum  $\Delta x/h$  values. Moreover, the wave setup continues to be very well predicted by the SPPhysics v.2 model everywhere (Makris et al. 2009). Correlation coefficients, portrayed in Fig.4 (right), are of the order of 0.9 and higher, in most test cases.

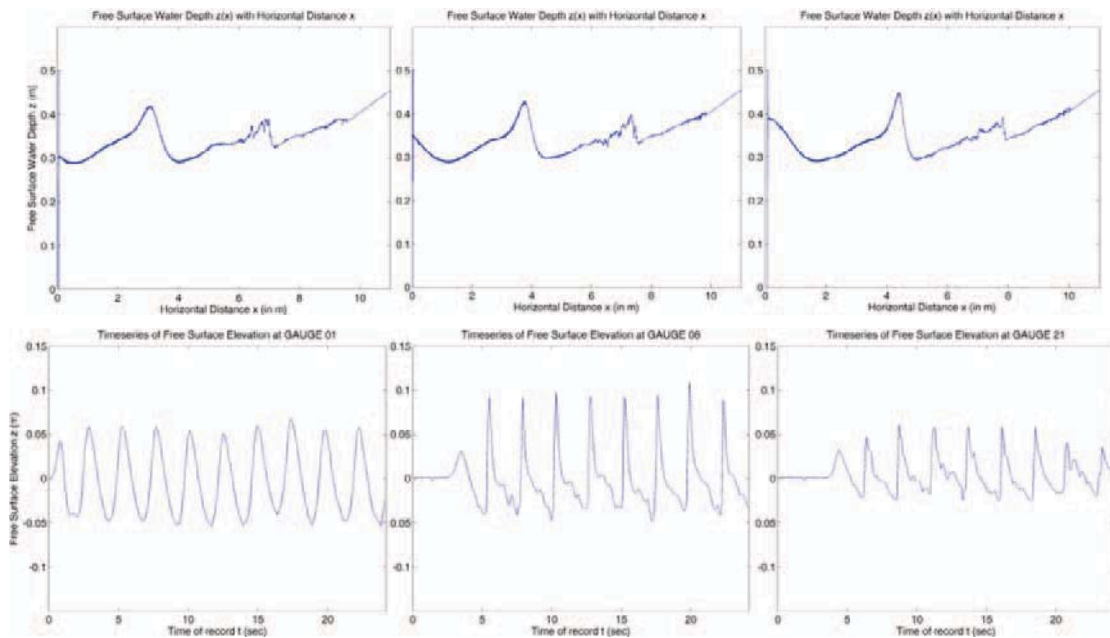


Figure 3: [Upper] SPPhysics free-surface elevation snapshots for simulation test case 13; [Lower] SPPhysics free-surface elevation time-series portrayal at specific gauges out of the surf zone [left], in the incipient breaking region [middle] and inner surf zone [right]

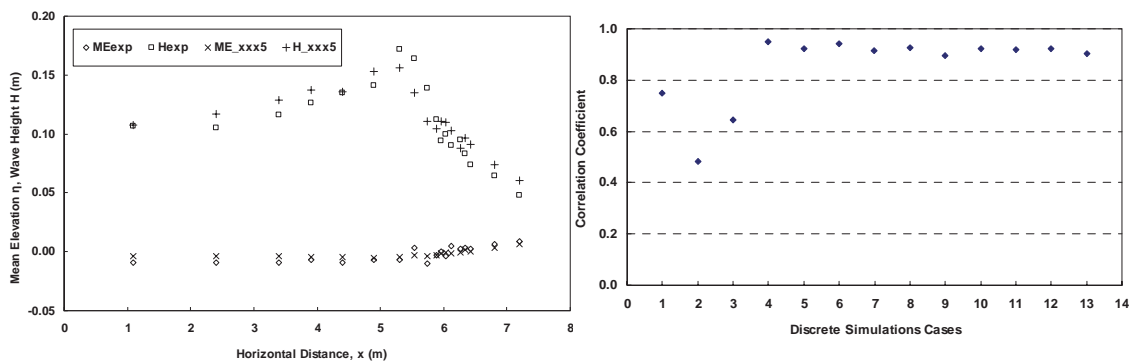


Figure 4: Wave height H and mean free-surface elevation ME distribution comparison between experiments (exp) and characteristic simulation test case 13 [left] - Correlation coefficients between experimental and simulation output for wave heights [right]

### 3.3 Free-surface elevation and depth-averaged velocities elaborate versions

In Fig.5 the root mean square (r.m.s.) values of the fluctuating free-surface elevation (left) and depth-averaged velocities (right) are given for Test case 12. Comparisons with the experimental respective values reveal striking coincidence (correlation coefficient 0.96) for the first and somewhat discrediting results for the second (correlation coefficient  $\sim 0.5$ ). This has probably something to do with the SPH model's inherent incapability to simulate correctly boundary layer effects, due to lack of water-solid friction modelling. That produces spuriously effects for the velocity field values near the solid boundaries. This is also discussed further below, concerning undertow simulation. The ensemble-averaged (Nadaoka et al., 1989) free-surface elevation (left) and depth-averaged velocities (right), in the outer (upper) and the inner (lower) surf zone, are presented in Fig.6. Very well agreement is pursued against SF05 results even in terms of raw values of our simulations, for all Test cases. Depth-averaged velocities, in deep or shear intensified regions like the breaking point, are a mild exception, likely due to the aforementioned reasons. In shallower regions accordance criteria are met, no matter the calibration.

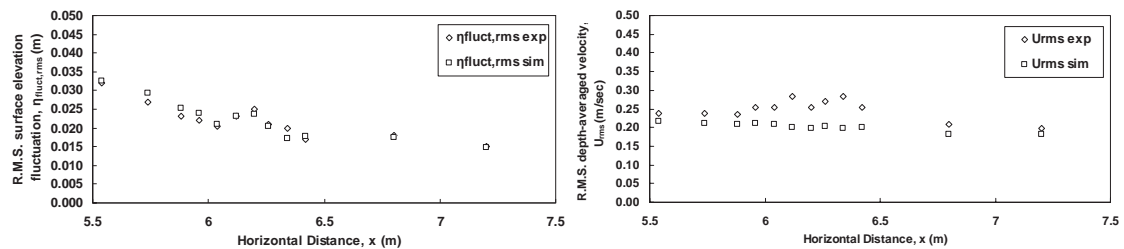


Figure 5: Comparison of experimental (square) and simulated (rhombus) r.m.s. values of free-surface elevation fluctuation [left] and depth-averaged velocities [right]

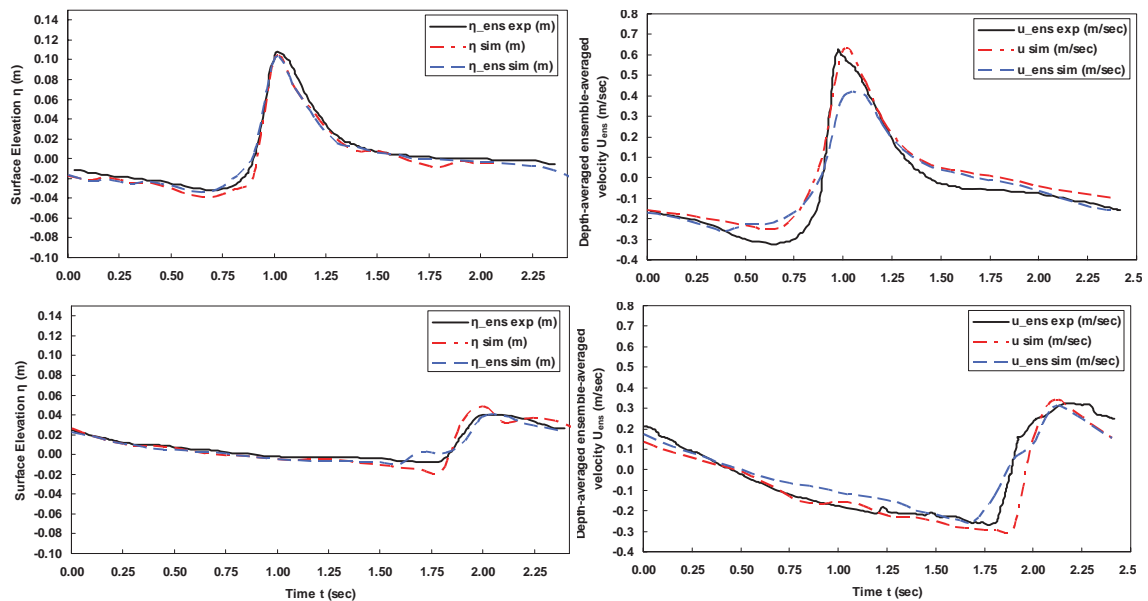


Figure 6: Comparisons of SF05 derived output data (full line) against simulation ones for ensemble-averaged (dashed line) and real-time (dash-dotted line) values of free-surface elevation [left] and depth-averaged velocities [right] at specific gauges in the incipient breaking region [upper] and the inner surf zone [lower]

### 3.4 Turbulent flow features (velocity Fourier power spectra - vorticity patterns)

The horizontal and vertical turbulent (fluctuating component) velocity Fourier spectra, derived by the simulated velocity field of Test case 6, at the incipient breaking region and still surface level are presented in Fig.7. Gradients of approximately  $-5/3$  (on the log/log scale), typical of isotropic (inertial sub-range) turbulence, and  $-3$ , typical of two-dimensional frozen turbulence, are sketched on the graphs (SF05). Improvement of results is evident, compared to Makris et al. (2010b), since the computed velocity power spectrum trend tails closely the  $-5/3$  gradient up to high frequencies, that correspond to SPS-treated small scale eddies. Refined resolution and

sufficient recording times contribute to this improvement. Despite that, the background gradient close to -3 still eludes even from our present analysis of enhanced resolution. The above only occur at still water level throughout the entire surf zone region. At mid-depth the statistically isotropic turbulence defining scaling law is concealed for nearly all frequency bands. In Fig.8 vortical periodic flow structures are shown in a two-dimensional vertical plane, from large-scale down to small-scale eddies. Coherent multiple vortical structures were evident during breaking, becoming elongated along the surface during bore propagation just as reported in SF05. A thick layer of positive vorticity from the free surface to trough level is apparent while a thin layer of counter-rotative vorticity prevails near the bed just as in SF05. At the end of the plunging region and following the bore, there were also concentrated regions of mean-valued vorticity. Simultaneously, persisting elongated structures of negative vorticity are observed at the toe of the roller, initially similar to a mixing layer. These coherent turbulent structures generated there together with multiple horizontal vortices shoreward of the crest were also clearly reported by SF05. The intense obliquely descending eddies (Nadaoka et al., 1989) seaward of the plunging wave crest cannot be identified yet, due to lack of three-dimensional effects. Preliminary respective results seem promising in future depicting of this kind of structures.

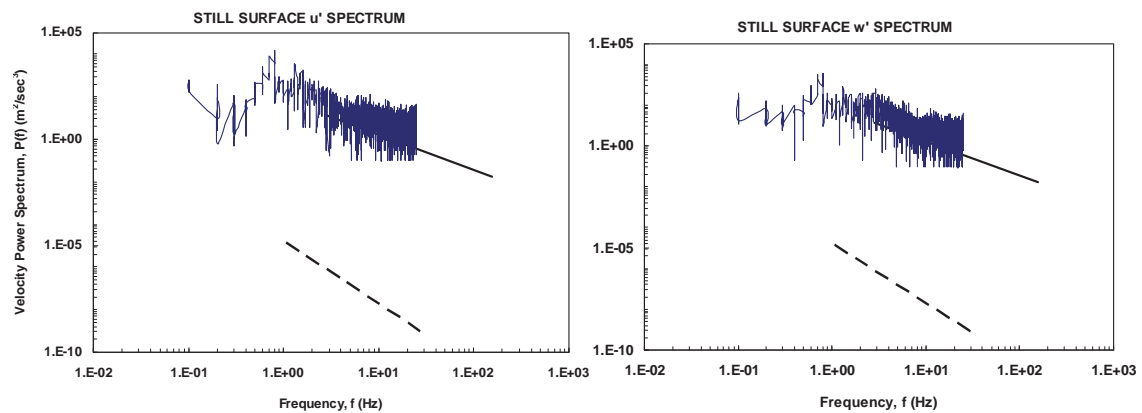


Figure 7: Fourier spectra of simulated horizontal [left] and vertical [right] turbulent velocity components for the incipient wave breaking region (Gauge 8) and large recording time (Test 6) at still-surface level. The  $-5/3$  (full line) and  $-3$  (dashed line) log-log gradients are also shown. Ensemble-averaging Nyquist filter is set to 25 Hz.

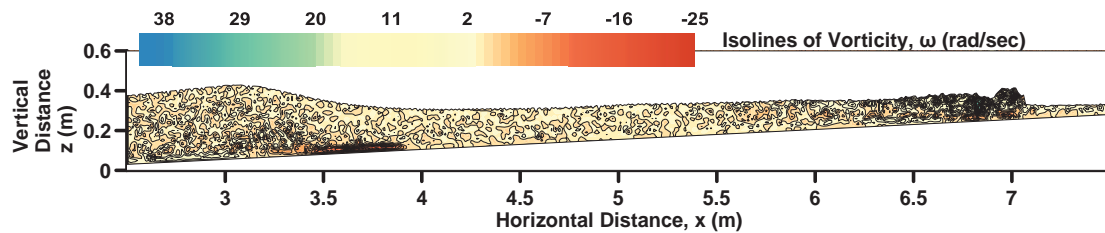


Figure 8: Simulated SPHysics vorticity field under plunging breaking waves and respective coherent structures and patterns of large-scale eddies

### 3.5 Wave-induced mean flows (Undertow and Stokes drift)

Period-averaged kinematics for the whole computational domain was also obtained (Test case 12 in Fig.9) showing shoreward mass transport above trough level (Stokes drift) and undertow below. Even the shoreward inversion of the undertow near the bed is well predicted. In general the vertically distributed time-averaged velocity follows a somewhat plausible trend, yet its depth-averaged value shows a questionable overall net shoreward propensity, where naught balance should exist. Non-linearity of propagating and breaking waves is also plausibly depicted, if the positioning of the setup level compared to the crest and trough envelopes is carefully observed (Fig.9), yet the undertow, although predicted, seems underestimated, as noted above. On the other hand, the Stokes drift is intensified in the breaking region causing considerable increase in momentum and mass transport and thus dramatic degradation of the crest envelope and consequent decrease in wave height, as deduced firstly by Nadaoka et al. (1989) and SF05.

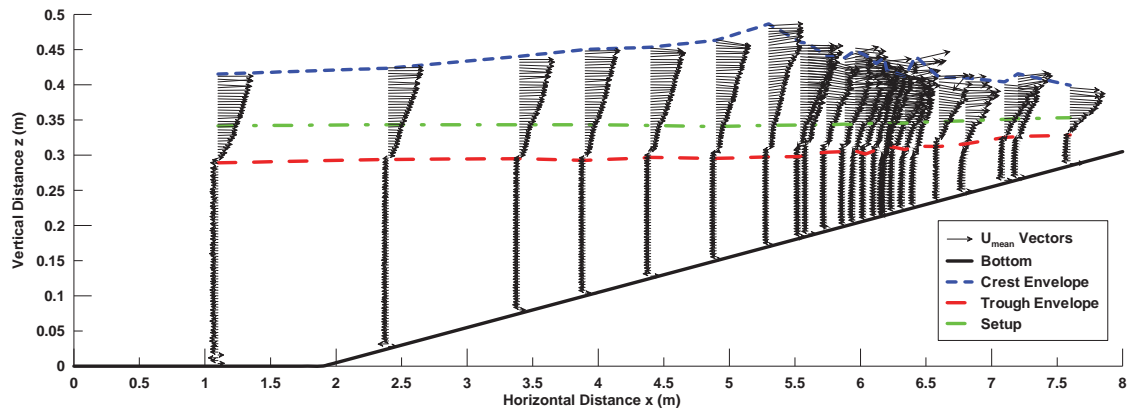


Figure 9: Time-averaged vertical distribution of velocity vectors at various gauges covering the whole computational field, clearly discriminating the lower (undertow) and upper (Stokes's drift) wave-induced mean flow regions defined by wave crest (small dashed line), trough (large dashed line) and wave setup (dash-dotted line) envelopes

## 4 Conclusions

The recently brought out SPHysics v.2 model combined with refined resolution calibration is put to the test against the experimental data of SF05. Following several past efforts with lean results, very good agreement was finally achieved for various simple and more sophisticated features concerning the hydrodynamics of plunging wave breaking, consequent surf zone turbulence and wave-induced mean flows. Spatial resolution turns out to be the most significant factor in forming plausible results for SPH simulations. An effort to bend the extremely time-consuming computations, moving towards 1~2 million particles, with the use of a new 'parallel' version of the SPHysics code is set as a future research goal.

## 5 References

- Dalrymple R. A.; Rogers B. D. (2006): Numerical modeling of water waves with the SPH method. In: Coastal Engineering, Vol. 53, pp. 141-147. ISSN 0378-3839.
- Gómez-Gesteira M.; Rogers B. D.; Dalrymple R. A.; Crespo A. J. C.; Narayanaswamy M. (2010a): User Guide for the SPHysics Code v2.0. <http://wiki.manchester.ac.uk/sphysics>.
- Gómez-Gesteira M.; Rogers B. D.; Dalrymple R. A.; Crespo A. J. C. (2010b): State-of-the-art of classical SPH for free-surface flows. In: Journal of Hydraulic Research, Vol. 48, Extra Issue, pp. 6–27. doi:10.3826/jhr.2010.0012.
- Makris C. V.; Memos C. D.; Krestenitis Y. N. (2009): Numerical simulation of near-shore wave breaking using SPH method, in: Proceedings of the 4<sup>th</sup> SCACR, – Int. Short Conference on Applied Coastal Research. ISBN 978-3-00-030141-4. Barcelona, Spain.
- Makris C. V.; Krestenitis Y. N.; Memos C. D. (2010a): SPH Numerical Simulation of Surf Zone Characteristics, in: Proceedings of 6<sup>th</sup> ISEH - International Symposium on Environmental Hydraulics, Vol. 1, pp. 445-450. ISBN 978-0-415-59545-2. Athens, Greece.
- Makris C. V.; Krestenitis Y. N.; Memos C. D. (2010b): SPHysics code validation against a near-shore wave breaking experiment, in: Proceedings of 5<sup>th</sup> SPHERIC - International SPH European Research Interest Community Workshop, pp. 245-252. Manchester, UK.
- Monaghan, J. J. (2005): Smoothed particle hydrodynamics. In: Rep. Prog. Phys., Vol. 68, pp. 1703-1759. ISSN 0034-4885.
- Nadaoka K.; Hino M.; Koyano Y. (1989): Structure of the turbulent flow field under breaking waves in the surf zone. In: J. Fluid Mech., 204, pp. 359-387.
- Stansby P. K.; Feng T. (2005): Kinematics and depth-integrated terms in surf zone waves from laboratory measurement. In: J. Fluid Mech., Vol. 529, pp. 279-310. doi: 10.1017/S0022112005003599